Formation and Reversible Dissociation of Coiled Coil of Peptide to the C-Terminus of the HSV B5 Protein: A Time-Resolved Spectroscopic Analysis

Ordel J. Brown,* Santiago A. Lopez,† A. Oveta Fuller,† and Theodore Goodson III*
*Department of Chemistry, University of Michigan; and †Department of Microbiology and Immunology, School of Medicine, University of Michigan, Ann Arbor, Michigan

ABSTRACT An understanding of the molecular mechanisms of the newly characterized herpes simplex virus (HSV) B5 protein is important to further elucidate the HSV cell entry and infection. The synthetic peptide of B5 (wtB5) was functionalized with the nonlinear optical chromophore cascade yellow and its molecular dynamics was probed at physiological and endosomal pH (pH 7.4 and 5.5, respectively). Steady-state CD spectroscopy was utilized to characterize the peptides at different pH. These spectra showed structural changes in the peptide with time measured over several days. Nonlinear optical measurements were carried out to probe the interactions and local environment of the labeled peptide, and the increase in the two-photon cross section of this system suggests an increase in chromophore-peptide interactions. Time-resolved fluorescence upconversion measurements reflected changes in the hydrophilic and hydrophobic local environments of the labeled peptide-chromophore system. Ultrafast depolarization measurements gave rotational correlation times indicative of a reversible change in the size of the peptide. The time-resolved results provide compelling evidence of a reversible dissociation of the coiled coils of the wtB5 peptide. This process was found to be pH-insensitive. The data from this unique combination of techniques provide an initial step to understanding the molecular dynamics of B5 and a framework for the development of novel imaging methods based on two-photon emission, as well as new therapeutics for HSV.

INTRODUCTION

Herpes simplex virus (HSV) types 1 and 2, are widespread human pathogens that infect a wide range of animal tissue. They establish lifelong latency in cells and recurrent infections result from periodic viral reactivation causing oral and genital lesions (1–3). HSV infection of cells requires fusion of the viral and cell membranes through the synchronized action of specific viral (gB, gC, gD, gH, and gL) and cell-surface proteins (heparin sulfate (HS) proteoglycans, nectin-1 and nectin-2, and herpes virus entry mediator (HVEM)) (1–7). The current working model for HSV entry into cells proposes that in the initial step, gB and gC interact with HS proteoglycans, facilitating virus-cell attachment. gD then binds to a receptor, facilitating membrane fusion mediated by gB and the gH/gL heterodimer (4–7). Recent reports outlined the structural characteristics of the C-terminus of gD and revealed that this region plays an important role in HSV entry (2,7). Paralleling this finding is the characterization of the 43-kDa protein B5, which is believed to be one of the cell-surface receptors that mediate HSV entry into cells via gD activation (7). Computational analysis showed that the C-terminus (amino acids 344–374) of B5 has a high probability of forming an α-helical coiled coil (7–9). This is particularly interesting, since computational modeling has also shown that it is highly possible that gH and gL form coiled coils (8–10).

Coiled coils are the oligomerization domains essential to the fusion of a number of viral and cell membranes. The coiled coil results from α-helices possessing a seven-residue (denoted *a–g*) repeat motif (8–11) of hydrophobic and hydrophilic residues. The hydrophobic residues occupy the *a* and *d* positions and generate a hydrophobic seam along which two or more helices align in parallel or antiparallel mode. The helices are stabilized by hydrophobic and ionic interactions (8–11). One of the criteria that established B5 as an HSV cell receptor is the inhibition of viral activity by synthetic peptides identical to its active region (8). Well-documented studies utilizing synthetic peptides to the coiled coil domains of viral proteins include those of human immunodeficiency virus retroviruses (12,13), parainfluenza viruses (14), Sendai virus (15) and paramyxovirus (16), and a 30-mer synthetic peptide to the B5 C-terminus, denoted wtB5, is reported to inhibit HSV activity (8,9). Current therapeutic strategies against HSV are aimed at viral DNA replication and are prone to inactivity due to the evolution of mutated drug-resistant virus strains. For the viruses that contain coiled coils, as in the case of human immunodeficiency virus, therapeutics that work at the site of action of the inhibitory synthetic peptides are being developed as antiviral agents. The functional C-terminus of the B5 or functional regions of its viral ligand, therefore, provide excellent antiviral targets (8). The ultimate development of ef fective therapeutics demands an in depth understanding of the structure and function of B5 and its associated viral ligand/s. Although mutagenesis and computer simulations have indicated that B5 affects infection of the cell by the HSV, and some structural properties have been elucidated (8), to date, a viral

Submitted November 15, 2006, and accepted for publication April 9, 2007.

Address reprint requests to Theodore Goodson III, Dept. of Chemistry, University of Michigan, Ann Arbor, MI 48109. E-mail: tgoodson@umich.edu.

Editor: Paul H. Axelsen.

0006-3495/07/08/1068/11 $2.00

doi: 10.1529/biophysj.106.100958

ligand for B5 is still undefined and the atomic structure of B5 or functional regions such as the C-terminus is unknown. There have been no reports of direct verification (biochemical or biophysical) that the B5 actually forms coiled coils and the molecular dynamics and mechanism of interactions are unclear (8,9).

Molecular dynamics of proteins and peptides are paramount to understanding their structure-function relationships (17–19). To probe the detailed interactions of the C-terminus and ultimately the function of the B5 protein, time-resolved and nonlinear optical measurements of wtB5 labeled with a fluorophore were carried out. These are sensitive methods that provide valuable information regarding fluorophore and peptide dynamics (20–25). Time-resolved fluorescence anisotropy, for instance, has been used to probe the rotational dynamics of peptides and proteins, providing insight into biophysical mechanisms through global and local motions of peptides via side-chain or extrinsic fluorophores (17–25). Analyses of the physical parameters associated with the motion and nonlinear optical properties of the fluorophore and fluorophore-labeled peptide allow for the elucidation of the molecular mechanisms associated with these changes. Herein, we report results from a detailed analysis of the wtB5 using a unique combination of steady-state, ultrafast spectroscopic, and nonlinear optical techniques, and we provide compelling evidence for reversible dissociation of the coiled coils at physiological and endosomal pH.

MATERIALS AND METHODS

Synthesis and characterization

The 30-amino-acid residue wtB5 peptide (8,9) was synthesized at the Protein Structure Facility at the University of Michigan.

Peptide labeling with fluorescent dye

We dissolved 5 mg of the wtB5 peptide in 0.8 mL of 0.1 M sodium bicarbonate buffer solution at pH 8.2 and 0.2 mL dry dimethylsulfoxide. The solution was gently stirred and kept on ice. We added 8.2 mg of cascade yellow succinimidyl ester (CY) in 0.1 mL dry dimethylsulfoxide to the peptide solution, and the reaction mixture gradually warmed to room temperature. This was then incubated overnight. Using MALDI-TOF mass spectrometry, 20-μL volumes were analyzed at 0, 2, and 24 h to follow the labeling process. We then added 65 μL of a 1.5 M hydroxylamine solution at pH 8 to the reaction mixture and stirred it for 2 h. The degree of labeling under these conditions was 63%.

Purification of conjugates

Low-molecular weight compounds and excess dye were separated from the labeled peptide by gel filtration chromatography. Bio-Gel P-6DG gel with an exclusion limit of 6000 D was used as the stationary phase on an econo-pac 10DG column from Bio-Rad (Hercules, CA). The fluorescent fractions were collected. Those showing absorbance at 280 nm and 405 nm were pooled and concentrated on a pretreated Microsep centrifugal device with a molecular-weight cut-off of 1K (Pall Life Sciences, East Hills, NY). The concentrated sample was freeze-dried and reconstituted with 500 μL acetic acid for HPLC analysis. HPLC purification was carried out at the Protein Structure Facility and MALDI-TOF mass spectrometry confirmed the identity of the peptide. The monolabeled conjugate was used in this study.

Steady-state spectroscopy

Ultraviolet (UV)-visible absorption spectra were recorded with a Hewlett-Packard (Palo Alto, CA) 8452A diode array spectrophotometer. Steady-state fluorescence measurements were performed on a SPEX (Edison, NJ) Fluorolog FL1T11 fluorimeter. The quantum yields were measured using a known procedure (26,27). Coumarin 307 was used as the standard. The absorbance was 0.03 or less. The solutions were purged with argon before measuring their emission spectra and the quantum yield was calculated using the following equation:

$$\phi_F = (\phi_F)_s \frac{\int J(\nu)d\nu (J_a)_s n^2}{\int J_s(\nu)d\nu J_a n_s^2},$$

where $(\phi_F)_s$ is the quantum yield of the standard; $\int J(\nu)d\nu$ is the area under the fluorescence emission curve for the sample; $\int J_s(\nu)d\nu$ is the area under the fluorescence emission curve for the standard; $(J_a)_s$ is the absorbance of the standard; J_a is the absorbance of the sample; n^2 is the refractive index of the solvent used for the sample; and n_s^2 is the refractive index of the solvent used for the standard.

Far-UV CD spectra were recorded in a quartz cell (1-mm path length) on an AVIV 202 series spectrophotometer in the range 190–250 nm at 298 K. At pH 7.4, samples were recorded in PBS buffer with 150 μM NaCl and pH 5.5 in sodium citrate buffer. Experiments were done in duplicate, and the concentration-dependent studies were performed in order both of increasing and of decreasing peptide concentration. The raw data were corrected for the buffer contributions by subtracting the buffer spectra. Ellipticity values (θ, deg) were converted to molar-residue ellipticity values ([θ], deg cm^2 dmol^{-1}), and molar-residue ellipticity ratios ($[\theta]_{222\ nm}/[\theta]_{208\ nm}$) were calculated.

Time-resolved spectroscopy

Time-resolved fluorescence measurements were carried out using a fluorescence upconversion set-up that has been described in detail in (28–30). The sample solution was excited with frequency-doubled light from a mode-locked Ti:sapphire femtosecond laser (Tsunami, Spectra Physics, Mountain View, CA) pumped by a Nd-YLF laser (Millenia X, Spectra Physics). This produces pulses of ~100 fs duration in a wavelength range of 385–430 nm. The polarization of the excitation beam for the anisotropy measurements was controlled with a Berek compensator. The horizontally polarized fluorescence emitted from the sample was upconverted in a nonlinear crystal of β-barium borate using a pump beam at ~800 nm that was first passed through a variable delay line. This system acts as an optical gate and enables the fluorescence to be resolved temporally. Spectral resolution was achieved by dispersing the upconverted light in a monochromator and detecting it using a photomultiplier tube (R1527P, Hamamatsu, Hamamatsu City, Japan).

Raw fluorescence anisotropy $R(t)$ was calculated from the decay curves for the intensities of fluorescence polarized parallel Ipar(t) and perpendicular Iper(t) to the polarization of the excitation light, according to the expression $R(t))(I\text{par} - GI\text{per})/(I\text{par} + 2GI\text{per})$. The factor G accounts for the difference in sensitivities for the detection of emission in the perpendicular and parallel polarized configurations. It was measured using perylene in methanol as a reference. In the real experiment, the G-factor has been found to be essentially unity (1.02 (0.02)).

Time-correlated single-photon counting (TCSPC) was performed using the second harmonic of the Kapteyn Murnane laser described below.

Two-photon absorption cross-sectional measurements

Two-photon cross-sectional methods were calculated using the two photon excitation fluorescence method as outlined in (28,31,32). We used 10^{-4}M

coumarin 307 in methanol as the standard reference, and a Kapteyn Murnane mode-locked Ti:sapphire laser with a bandwidth of 47 nm at 800 nm and pulse duration of 30 fs. A polarizer was used to vary the laser input power and an iris placed before the polarizer ensured a circular beam. A lens with focal length of 11.5 cm focused the laser beam on the sample cell. The fluorescence was collected perpendicular to the incident beam. A plano-convex lens directed the collected fluorescence into a monochromator. The output from the monochromator was coupled to a photomultiplier tube. Collected photons were converted to photon counts by a photon counting unit. A logarithmic plot between collected fluorescence photons and input intensity gave a slope of 2. This confirmed a quadratic relationship, and the two-photon-absorption cross section was calculated from the intercept.

RESULTS

Steady-state analysis

Absorption spectra of the free dye CY, wtB5, dye-peptide mixture (CY-wtB5), and labeled conjugate (CYwtB5) at pH 7.4 and pH 5.5 were recorded in the range 200–700 nm. The wtB5 showed characteristic maxima at 220 nm and 280 nm (data not shown). The spectrum of CYwtB5 showed a peak at 405 nm compared to 398 nm for CY and CY-wtB5 (Fig. 1). The bathochromic shift of the low energy peak, along with the increased intensity for CYwtB5, confirm conjugation of the fluorophore to the peptide (33). These effects result from the change in geometry of CY upon conjugation. The aromatic backbone of CY becomes more planar (22) and allows for greater π conjugation and substantial electron delocalization over the entire molecule. There are no such geometrical modifications in the case of the peptide-dye mixtures and therefore no significant perturbation of the electronic absorption spectra. The decrease in intensity of the absorption bands at low pH is most likely due to the acidification of residues in the peptide backbone and/or the fluorophore, which could result in mitigation of the intermolecular interactions.

The fluorescence intensity of CY, CY-wtB5 mixture, and labeled CYwtB5 is shown in Fig. 2. The fluorescence

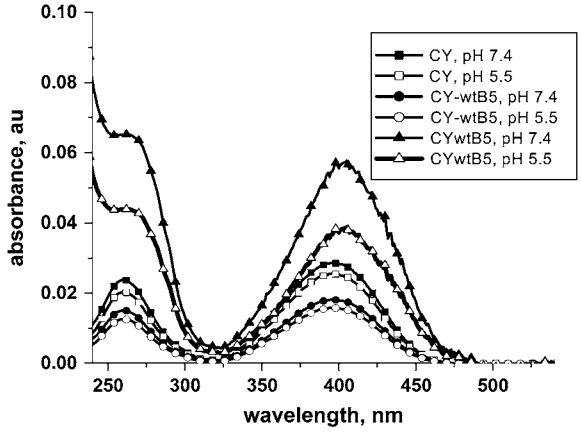

FIGURE 1 UV-visible spectra of 50 μM CY, CY-wtB5 mix, and labeled CYwtB5 at pH 7.4 and pH 5.5.

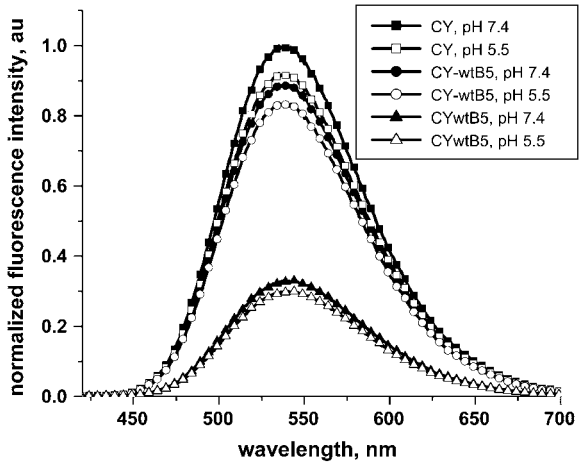

FIGURE 2 Normalized emission spectra of 50 μM CY, CY-wtB5 mixture, and labeled CYwtB5 at pH 7.4 and pH 5.5.

intensity of CY decreases upon interaction with wtB5 and the decrease is more pronounced when it is covalently bound to wtB5. This may result from the interaction of CY with quenchers such as the aromatic amines of the peptide backbone. The high internal flexibility of the peptide as well as the resultant geometry change in CY could facilitate these interactions. The fluorescence intensity of the systems (CY-wtB5 and CYwtB5) changed over time, and the rate of the change was concentration-dependent. The labeled peptide (50 μM) and a 1:5 dye/peptide mixture (50 μM peptide) showed a nonmonotonic change in fluorescence intensity over a period of approximately 90 days. The mixture at a 1:200 molar ratio (2 mM peptide), however, showed the nonmonotonic change over only 14 days. For instance, the fluorescence of CY decreases upon the initial mixing with wtB5 followed by a gradual increase up to 4 days, after which the intensity of the fluorescence decreases over 10 days.

To study the structural characteristics of the peptide and the effect of covalent and noncovalent binding of the dye, wtB5, CY-wtB5, and CYwtB5 were analyzed by far-UV CD spectroscopy. The far-UV CD spectra show minima centered at ~222 nm and 208 nm, characteristic of the presence of α- helices (Fig. 3), and indicate that the presence of the dye does not alter the secondary structure of the peptide. The shape of the spectra at pH 7.4 and pH 5.5 are similar, with a slight dampening of signals at lower pH. The ellipticity ratio (9,26,27) for wtB5, CY-wtB5, and CYwtB5 changed over time, and the rate of change depends on the peptide concentration. The rate of change for 2 mM wtB5 is shown in Fig. 4 and represents the common trend observed in all cases. It shows an interchange of the ellipticity ratios between average values of 1 and 0.85. The molar ellipticity, $[\theta]_{222\ nm}$, is concentration-dependent, and results are given in Figs. 5 and 6.

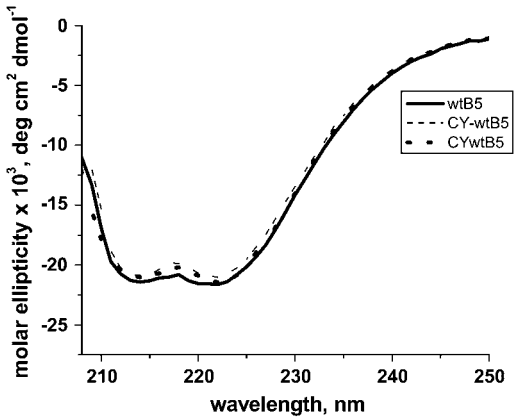

FIGURE 3 CD spectra of 50 μM wtB5, CY-wtB5 mixture, and labeled CYwtB5 in PBS buffer at pH 7.4.

Time-resolved fluorescence and two-photon absorption measurements

Time-resolved lifetime measurements

Even though CD spectroscopy has been extensively used to study α-helices and coiled coils of peptides, the technique by itself is inconclusive (34–39). Thus, we used ultrafast upconversion and TCSPC techniques, along with two-photon absorption measurements, to further analyze the behavior of the wtB5 peptide. These techniques provide sensitive and real-time information (17–25) that cannot be determined using CD spectroscopy (40,41). The fluorescence intensity decays (Fig. 7) determined from upconversion measurements were fitted with two exponentials and the lifetimes are given in Table 1. The short lifetime of ~2 ps was common to all the systems studied and the long lifetime (~400 ps) was resolved using TCSPC. These results gave intensity decays that were also fitted with a biexponential function. The longer lifetime of ~3 ns was unchanged in all the fluorescent systems and reveals insensitivity to the environment. The shorter lifetime, on the other hand, revealed some degree of sensitivity to the local environment, as is evident from the resulting decrease upon binding (covalently and noncovalently) to the peptide (Table 1).

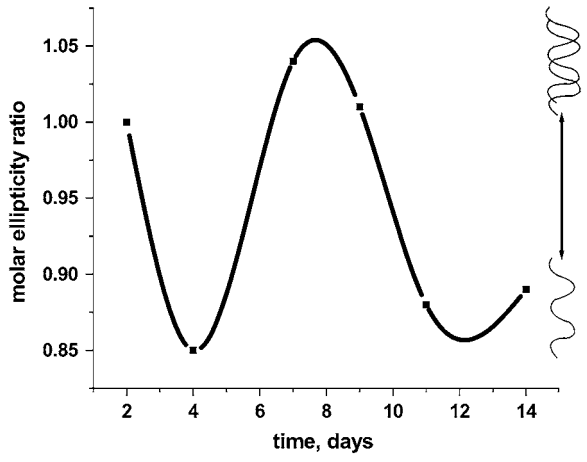

FIGURE 4 The changes in the ellipticity ratio of 2 mM wtB5 at pH 7.4 over time. The line is a visual aid to highlight the trend and the arrow shows possible interchange between α-helix and coiled coil.

The change in quantum yields for CY, CY-wtB5, and CYwtB5 (Table 1) implies significant differences in the fluorescence lifetimes of the free dye and the labeled peptide. However, this was not observed, as the approximately eight-fold decrease in the quantum yield of CYwtB5 (0.05) compared to CY (0.39) and CY-wtB5 (0.36) was not reflected in their lifetimes. This observation hints at the operation of complex excited-state interactions, and the disparity could arise from either of two scenarios (42). In the first instance, fluorescence quenching occurs before relaxation to the ground state. After excitation, there is rapid relaxation to a prefluorescent excited state, and the depopulation of this state is rather slow. A dye-peptide interaction strong enough to compete with the excited-state relaxation would result in quenching of the excitation energy before the prefluorescent state is reached. In the second case, it could result from a heterogenous mode of quenching. This involves a dark species that absorbs energy but relaxes to the ground state via an efficient nonradiative process (42).

Tables 2–4 summarize the time-dependent fluorescence lifetime data for CYwtB5 and CY-wtB5. The lifetimes changed nonmonotonically, at a concentration-dependent rate, and samples at millimolar concentrations changed faster than those at micromolar concentrations. The lifetime of the free dye in the PBS buffer did not change as a function of time, and within the limits of experimental accuracy, the average lifetimes determined at pH 5.5 and 7.4 were similar (Tables 2–4).

Time-resolved anisotropy measurements

The rotational correlation times of the fluorophore determined from time-resolved anisotropy experiments relate to overall rotational diffusion of the peptide and intramolecular motions of the peptide and attached fluorophore (43–46). The time-resolved anisotropy decays were best fitted with single exponentials (Fig. 8), and Table 1 shows values for the rotational correlation times at pH 7.4. There is a slight increase in the rotational correlation time of CY-wtB5 (254 ps) and CYwtB5 (220 ps) compared to the free dye (200 ps). Based on the timescales of the observed motions, the longer rotational correlation time for CY-wtB5 and CYwtB5 can be attributed to the intramolecular motions associated with the peptide backbone. In the case of CYwtB5, this may result from restricted movement about the lysine side chain (43,46).

The rotational correlation time changed significantly over time (Tables 2–4). The nonmonotonic change is concentration-dependent, and possibly due to a change in the local unwinding of the coiled coil of the peptide (47). The initial

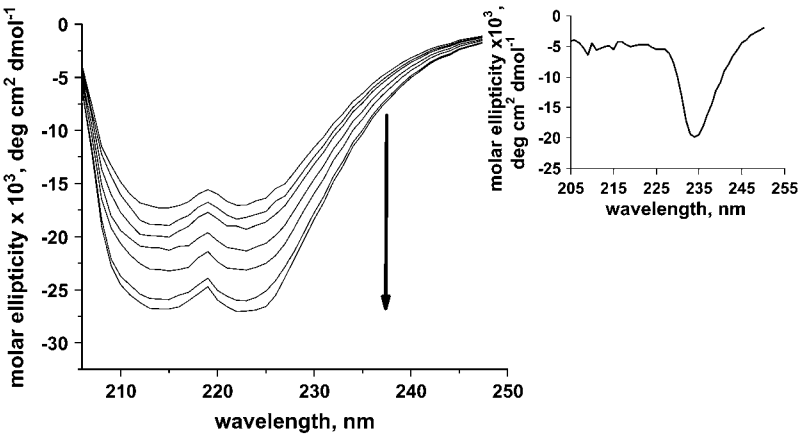

FIGURE 5 The CD spectra of increasing concentration of wtB5 at pH 7.4. The arrow indicates order of increase from 30 μM to 300 μM. (*Inset*) CD spectrum at 2 mM.

decrease may be a result of the dissociation of the coiled coil of wtB5, whereas the increase in rotational correlation time may be due to the association or recoiling of the individual α-helices. The timescales and the trend in the changes of the rotational correlation time were similar for CYwtB5 and CY-wtB5, and it can therefore be inferred that the same changes are being detected in both scenarios. Collectively, these results strongly suggest a reversible dissociation of the coiled coils of the wtB5 peptide at pH 7.4 and pH 5.5.

Two-photon absorption measurements

The two-photon measurements allow for the probing of detailed molecular interactions that cannot be done with one-photon measurements (48,49). The fluorescence from two-photon excitation is similar to that from one-photon excitation, with a maximum centered at 540 nm (data not shown). For all the systems studied, a logarithmic plot of the photon flux versus input intensity gives a slope of 2 and implies a two-photon excitation mechanism (31,50). A representative plot is shown in Fig. 9. Two-photon absorbance cross sections for CY, CY-wtB5, and CYwtB5 are given in Table 1. The drastic increase in the two-photon cross section of the labeled peptide results from the covalent interaction of the wtB5 and the CY. Conjugation of the dye to the peptide causes the low-energy band in the electronic absorption spectrum to be red-shifted due to an increase in the electronic delocalization over the system. This leads to an increase in intramolecular interactions such as charge-transfer reactions and/or transition dipole moments (27,31,50) as will happen when the aromatic rings of CY are made more planar upon conjugation to wtB5.

DISCUSSION

The wtB5 forms coiled coils with very weak interactions that dissociate reversibly at physiological and endosomal pH

Recent reports have shown that the B5 protein has a high propensity to form coiled coils and favors the formation of

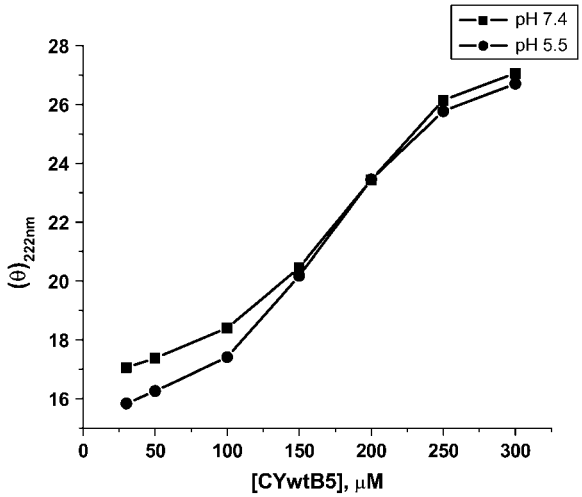

FIGURE 6 Plot of the molar ellipticity at 222 nm versus concentration of CYwtB5 at pH 7.4 and pH 5.5.

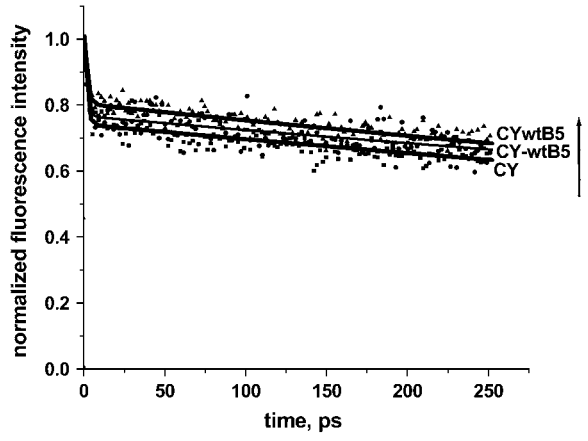

FIGURE 7 Normalized fluorescence intensity decays of 50 μM CY, CY-wtB5, and CYwtB5 in PBS at pH 7.4. Solid lines show best fit to multi-exponential functions.

TABLE 1 Photophysical and nonlinear optical parameters

System	$\lambda_{max,}$ (nm)	τ, ps	ϕ, ps	η	δ, GM
CY	398	1.58 ± 0.27 425 ± 32 3130 ± 40	200 ± 5.4	0.39	9.56
CY-wtB5 mix	398	1.16 ± 0.31 391 ± 40 3071 ± 44	254 ± 10	0.36	10.47
CYwtB5	403	1.77 ± 0.34 347 ± 29 3040 ± 33	219 ± 4.3	0.05	75.35

τ, fluorescence lifetime; ϕ, rotational correlation time; η, quantum yield; δ, two-photon cross-section in Göppert-Mayer (GM).

dimers, trimers, and tetramers at physiological pH (8,9). Although the cell receptors of the HSV, along with their many viral ligands, have been extensively studied, the molecular interactions governing the actual fusion and entry of the virus into cells are still not clearly understood.

The circular dichroism spectra of wtB5, CY-wtB5, and CYwtB5 reveal that the peptide forms coiled coils with weakly associated units. Results of the concentration-dependent studies of wtB5 are shown in Figs. 5 and 6. The increase in helical content, indicated by the increase of $[\theta]_{222\ nm}$, is consistent with an increasing number of coiled-coil structures formed at higher peptide concentrations (51–53). The sigmoidal relationship (Fig. 6) is consistent with the formation of very weak (51,52) intermolecular associations at higher concentrations (53). The dependence of the helical content on concentration was similarly observed in the case of CY-wtB5. The coiled-coil stability depends on such factors as helical propensity, hydrophobicity of the core residues, packing of residues in the core, electrostatic interactions adjacent to the core, and chain length (51). Particular amino acid residues have been shown to destabilize the coiled coil. These include tyrosine (Tyr), tryptophan (Trp) and asparagine (Asn) (52), and the destabilizing effect of these residues (8,9) in the core of wtB5 (Fig. 10) is confirmed from our results. Changes in the time-dependent spectra were surprising and implied an interchange between an α-helix and a coiled coil motif. The molar ellipticity ratio, $[\theta]_{222\ nm}/[\theta]_{208\ nm}$ tells whether the helix is monomeric or forms a coiled coil (9,26,27). Our results showed that the ellipticity ratio was interchangeable between average values of 0.85 and 1, reflecting a transition between these two forms. The relative structural simplicity of the coiled coil belies its varied functions in numerous proteins (34,54), and their molecular function is associated with the unwinding and unfolding of the coiled coil. For instance, Wang et al. (55) showed that the nanomechanical operation of myosin is associated with the reversible and irreversible dissociation and unwinding of the coiled coil structure. Carr and Kim (56) and Leikina et al (57) highlighted coiled coils uncoiling in the membrane fusion activities of hemagglutinin of the influenza virus. Hodges and colleagues (51) demonstrated that the unzipping or unwinding of coiled coils in kinesin is associated with its molecular function. Woehlke et al. (47) also alluded to the alternating of a coiled coil structure and a molten conformation in the kinesin function. The molecular mode of action of wtB5 may therefore rely on the observed reversible dissociation of its coiled coil. Reversible and irreversible dissociation of coiled coils as a function of pH, temperature, and denaturant concentration have been widely studied. The behavior of the wtB5, however, is most fascinating, reflecting a concentration-dependent, spontaneous, reversible dissociation process.

HSV infects a variety of cell types and the entry of the viral components into the host cells may operate via multiple cellular pathways. One of the most important factors of biological systems is pH, and both pH-dependent and pH-independent mechanisms of cell entry have been proposed (8,9,11). The effect of pH on the spectroscopic properties of CYwtB5 and CY-wtB5 was investigated. The systems were studied at pH 7.4 (physiological) and pH 5.5 (endosomal). The steady-state and time-resolved measurements of the labeled peptide and dye mixtures at pH 7.4 are tantamount to the results at pH 5.5, which reveals that the behavior of wtB5 is insensitive to the pH studied. This is consistent with the hypothesis put forward by Fuller et al. (8,9), and points to the operation of a pH-independent mechanism.

Under all the conditions studied, the rotation of the fluorophore is independent or uncoupled from the rotation of the peptide molecule. This is evident from the absence of a long rotational correlation time, reflecting the rotational diffusion of the wtB5 peptide, and may be due to the limited spectroscopic properties of CY. Global motion of the wtB5 peptide containing 30 amino acids is expected to take place on a timescale >20 ns. The lifetime of the fluorescent probe (~3 ns) may be too short to detect and report the expected global motions. The rotational diffusion of the peptide is

TABLE 2 Photophysical parameters for systems at 50 μM and pH 7.4, τ and ϕ in ps

	CY-wtB5				CYwtB5			
Day	τ_1	τ_2	ϕ	η	τ_1	τ_2	ϕ	η
0	3.96 ± 1.10	532.76 ± 36.7	200.65 ± 17.51	0.22	3.87 ± 1.01	567.07 ± 56.70	211.09 ± 7.66	0.038
21	3.28 ± 0.97	686.09 ± 54.72	312.44 ± 17.88	0.21	3.38 ± 0.91	638.38 ± 42.17	304.96 ± 18.76	0.04
45	1.99 ± 0.84	462.31 ± 19.66	226.66 ± 15.01	0.22	2.84 ± 0.81	503.61 ± 19.09	209.14 ± 15.07	0.032
68	4.53 ± 1.05	593.71 ± 38.22	299.36 ± 13.65	0.25	2.97 ± 0.94	602.43 ± 31.87	316.03 ± 18.28	0.035
92	3.17 ± 1.01	512.22 ± 26.72	201.71 ± 12.58	0.23	3.30 ± 1.01	601.53 ± 40.12	214.04 ± 13.73	0.037

TABLE 3 Photophysical parameters for systems at 50 μM and pH 5.5, τ and ϕ in ps

	CY-wtB5				CYwtB5			
Day	τ_1	τ_2	ϕ	η	τ_1	τ_2	ϕ	η
0	3.96 ± 1.10	532.76 ± 36.74	218.47 ± 13.01	0.21	3.87 ± 1.01	567.07 ± 56.70	217.49 ± 20.12	0.04
21	3.28 ± 0.97	686.09 ± 54.72	310.20 ± 23.87	0.22	3.38 ± 0.91	638.38 ± 42.17	302.76 ± 19.38	0.038
45	1.99 ± 0.84	462.31 ± 19.66	222.32 ± 19.56	0.25	2.84 ± 0.81	503.61 ± 19.09	214.14 ± 18.62	0.035
68	4.53 ± 1.05	593.71 ± 38.22	315.38 ± 17.87	0.22	2.97 ± 0.94	602.43 ± 31.87	301.27 ± 12.44	0.032
92	3.09 ± 1.01	630.41 ± 56.69	202.21 ± 10.01	0.23	3.21 ± 1.06	617.24 ± 42.51	288.33 ± 12.74	0.037

therefore uncoupled from the dye (43) and the reorientational dynamics of the dye is dominated by contributions from intramolecular motions. Even though the fluorescence lifetime of CY is insufficient to facilitate the accurate determination of the rotational correlation time of the whole peptide, its time-resolved anisotropy decay can be used as a measure of peptide interaction, that is, coiled coil dissociation and association through the determination of local motion (58). The nonmonotonic change in the rotational correlation times observed for the wtB5 during 14 days indicates reversible changes in the size of the peptide with time. This is further corroborated by results from the CD spectra. Over time, the CD spectrum changes (Figs. 6 and 7) to reflect changes in the ellipticity ratios that are consistent with the dissociation and association of coiled coils (58,59). This trend was observed for peptide concentrations in the micromolar and millimolar range. At millimolar concentration, the peptide is initially aggregated. It is therefore tempting to infer that the changes in rotational correlation time may be due to a reversible aggregation process. The results from the studies done at micromolar concentrations (Tables 2 and 3) dispel this view, however, as the change in the rotational correlation time paralleled that at micromolar concentrations. Additional proof also stems from the comparable timescales. A noteworthy feature is the absence of the very long rotational correlation time (>400 ps) in the case of the peptide at micromolar concentration. At micromolar concentrations, the peptide is nonaggregated and the changes are most likely due to an interplay between the coiled coil and monomeric forms. It is also interesting to note that after the initial dissociation of the aggregated species, the peptide does not revert to the aggregated state. Since aggregation was shown to be concentration-dependent, it is tempting to conclude here that the concentration changes after the initial aggregate dissociation. This was not the case, however, since the UV-visible spectrum confirmed no concentration changes. This locking of the peptide in a state where it dissociates reversibly between a coiled coil and a monomer even at millimolar concentrations that promote aggregation is surprising and might be paramount to the molecular function of B5. It therefore warrants further investigation. No such changes were observed in the case of the free dye. Taken together, these results show that the rotational correlation time of ~450 ps is due to the motion from the aggregated peptide. The fluorophore is in a restricted environment and does not have much freedom of movement. The motion of the coiled coil and α-helical monomer accounts for the rotational correlation times of ~300 ps and ~200 ps, respectively. These findings are consistent with the expectation that there is more freedom of movement in the monomeric species compared to the coiled coil and aggregates. Again, the kinetics of dissociation of wtB5 may be linked to its biochemical function and the mechanism of HSV infection, and it requires more detailed study.

The time-dependent results of the time-resolved lifetime measurements of CYwtB5 and CY-wtB5 (Tables 2–4) show changes in the microenvironment of CY. Since the lifetime of the fluorophore depends on the hydrophobicity of its local environment, the nonmonotonic change in the fluorescence lifetimes may be due to the fluorophore experiencing an interchange between a hydrophilic and hydrophobic environment (25,33). This may result from the association and dissociation of the wtB5 α-helix. At 50 μM, the wtB5 is monomeric and forms aggregates at 2 mM. The initial decrease in the fluorescence lifetimes (Table 4) is perhaps the result of the gradual transition from a ''closed'' peptide

TABLE 4 Photophysical parameters of 2 mM CY-wtB5 over 14 days, τ and ϕ in ps

	CY-wtB5mix, pH 5.5				CY-wtB5mix, pH 7.4			
Day	τ_1	τ_2	ϕ	η	τ_1	τ_2	ϕ	η
0	5.18 ± 1.77	1236.55 ± 94.43	462.70 ± 33.87	0.04	3.19 ± 0.81	1308.96 ± 99.02	429.15 ± 29.83	0.22
2	3.96 ± 1.10	710.8 ± 67.37	298.74 ± 23.07	0.037	3.77 ± 1.05	675.57 ± 60.41	303.7 ± 24	0.22
4	1.88 ± 0.85	423.11 ± 18.81	208.65 ± 15.27	0.033	1.86 ± 0.88	442.02 ± 20.69	196.86 ± 14.29	0.23
7	2.98 ± 0.62	547.3 ± 19.41	315.50 ± 17.99	0.035	3.48 ± 0.91	550.38 ± 20.03	311.8 ± 16.76	0.23
9	9.09 ± 1.52	870.69 ± 5.86	328.91 ± 19.23	0.04	6.17 ± 0.86	827.24 ± 47.34	333.73 ± 19.23	0.22
11	4.15 ± 0.81	392.83 ± 12.34	215.74 ± 12.77	0.038	3.70 ± 0.70	344.30 ± 9.68	217.38 ± 9.12	0.17
14	3.67 ± 4.57	607.89 ± 27.86	292.38 ± 9.25	0.036	22.37 ± 4.76	1097.05 ± 246.98	121.71 ± 8.55	0.08

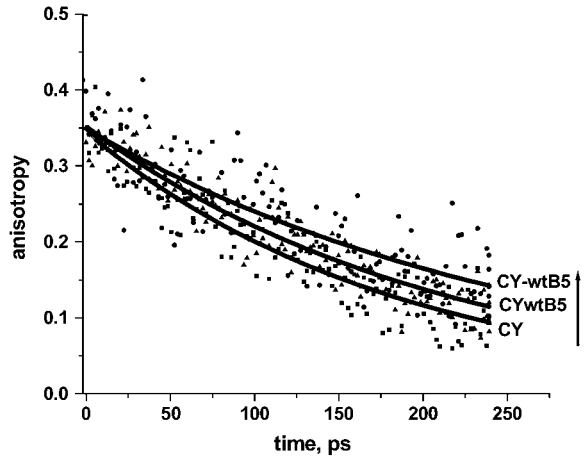

FIGURE 8 Time-resolved fluorescence anisotropy decays for 50 μM CY, CY-wtB5, and CYwtB5 in PBS at pH 7.4. Solid lines show best fit to mono-exponential functions.

structure to a more ''open'' configuration, as can occur upon deaggregation of wtB5. The increase in the lifetime would then be due to unwinding of the coiled coil.

There is a rapidly increasing trend in the use of novel microscopic techniques based on nonlinear optical phenomena such as two-photon excited fluorescence in biological imaging (48). Molecules that are ideal for use in these imaging techniques are those with a large two-photon absorption cross section (27,31,49,50,60–62) and this two-photon absorption process is confirmed by the quadratic dependence of the two-photon fluorescence intensity on the laser intensity. A representative plot for CYwtB5 is shown in Fig. 9. The significantly larger two-photon cross section of CYwtB5 therefore indicates that CYwtB5 is a very good

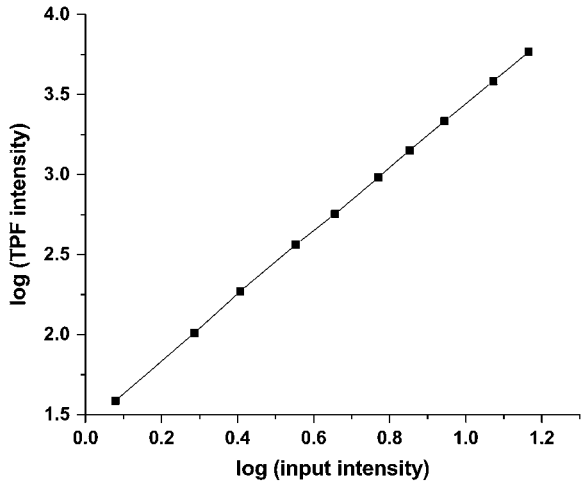

FIGURE 9 Plot of log (TPF intensity) versus log (input intensity) for 50 μM CYwtB5. (See Materials and Methods). TPF, two-photon fluorescence.

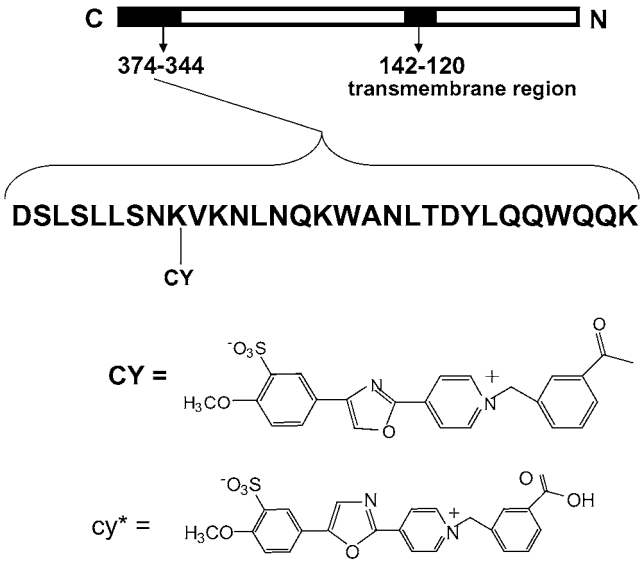

FIGURE 10 Diagrammatic representation of the B5 protein, the C-terminus (amino acids 344–374), cascade yellow (*CY*) attached to the peptide and the hydrolyzed product (*cy**) used in CY-wtB5 mix.

specimen for in vitro two-photon-excitation fluorescence imaging. With higher resolution and 3-D imaging coupled with the ability to image at greater sample depths, this technique far exceeds the conventional confocal microscopic methods. Also, the problem of photodamage that is frequently encountered in conventional microscopic techniques is greatly reduced, since the excitation radiation used in two-photon excitation fluorescence microscopy is in the near-infrared region. Added to this, CY is biocompatible with wtB5: the CYwtB5 is water soluble and does not form aggregates at physiological conditions.

Implications for viral fusion and entry

We have used a unique combination of steady-state and ultrafast spectroscopic and nonlinear optical techniques to study the wtB5 peptide of the recently characterized HSV B5 protein. These types of molecular dynamics studies compliment bioassays and steady-state biophysical studies and can give information on the molecular mechanisms of B5 even in the absence of detailed structural information. The existence of reversible conformational changes may be critical in HSV viral fusion and entry. The mechanism of HSV entry into the cell proposed by Fuller at al. (8,9) occurs at physiological pH and is pH-independent. These same conditions also promote the reversibility of the coiled coil formation of B5.

Since coiled-coil domains normally reflect the oligomerization state of their full-length proteins, they present the advantage of structure and function analysis without obstacles such as supramolecular assembly, which is associated with full-length proteins. The main function of coiled coils is the oligomerization of individual α-helices, and they possess

hydrophobic seams along which two or more helices align in parallel or antiparallel mode (53,63–65). Oligomerization is essential in a myriad of cellular functions since it generates a high local concentration of functional sites and allows the concerted operation of clustered domains (57). The observed reversible dissociation may imply the regeneration of wtB5 after fusion of the viral and cell membranes. A number of scenarios can now be envisaged. The interaction of the viral ligands containing coiled coils with the coiled coils of the B5 brings about conformational changes that concentrate the B5 protein at the contact zone. This is similar to the mechanism predicted for hemagglutinin of the influenza virus (56,66). Conversely, the interaction of gD with one of its cell receptors could elicit the conformational changes that concentrate B5 protein at the contact zone through self-association of the B5 coiled coils. After fusion, B5 reverts to a monomeric α-helix, allowing for further interactions. These propositions further lend credence to a pH-independent mode of action of the HSV. Even though these studies provide much needed information on the newly discovered B5 protein, there are still a number of questions to be answered and mechanisms to elucidate to fully understand the molecular dynamics of the B5. These include, for instance, information on the mutation-related inhibition mechanism, details on the kinetics of the reversible dissociation, the specific viral ligands that B5 engages, and the process by which this is done. Work continues in our laboratories with the aim of answering these questions. Notwithstanding this, however, we have provided exciting new insights into the molecular dynamics of the wtB5 of HSV B5.

CONCLUDING REMARKS

Using very sensitive ultrafast spectroscopic methods, we have shown the unusual behavior of wtB5. Photophysical parameters determined from nonlinear optical measurements also highlight the in vitro fluorescence imaging potential of labeled wtB5. The question of whether or not B5 forms coiled coils (8,9) has been answered, but even more interestingly, we have provided evidence that the coiled coils reversibly dissociate at physiological and endosomal pH. We believe that these results are important in the elucidation of the overall mechanism of HSV fusion and entry into host cells. They provide the initial critical details of the molecular dynamics of wtB5. They also concur with a pH-independent mechanism for viral fusion and entry and indicate that the coiled coils of B5 may operate in such a way as to concentrate the protein at the point of contact of the virus. This may occur through a combination of processes that involve fusion of the viral and cell membranes via the self-association and/or interaction of B5 coiled coils with the coiled coils of the viral ligand. A recent study showing that the wtB5 has a relatively high probability of fusion (67) further supports these propositions.

REFERENCES

1. Tamm, L. K., X. Han, Y. Li, and A. L. Lai. 2002. Structure and function of membrane fusion peptides. *Biopolymers*. 66:249–260.
2. Cocchi, F., D. Fusco, L. Menotti, T. Gianni, R. J. Eisenberg, G. H. Cohen, and G. Campadelli-Fiume. 2004. The soluble ectodomain of herpes simplex virus gD contains a membrane-proximal pro-fusion domain and suffices to mediate virus entry. *Proc. Natl. Acad. Sci. USA*. 101:7445–7450.
3. Spear, P. G. 2001. A first step toward understanding membrane fusion induced by herpes simplex virus. *Mol. Cell.* 8:2–4.
4. Spear, P. G. 2004. Herpes simplex virus: receptors and ligands for cell entry. *Cell. Microbiol.* 6:401–410.
5. Carfı, A., S. H. Willis, J. C. Whitbeck, C. Krummenacher, G. H. Cohen, R. J. Eisenberg, and D. C. Wiley. 2001. Herpes simplex virus glycoprotein D bound to the human receptor HveA. *Mol. Cell.* 8:169–179.
6. Krummenacher, C., V. M. Supekar, J. C. Whitbeck, E. Lazear, S. A. Connolly, R. J. Eisenberg, G. H. Cohen, D. C. Wiley, and A. Carfi. 2005. Structure of unliganded HSV gD reveals a mechanism for receptor-mediated activation of virus entry. *EMBO J.* 24:4144–4153.
7. Perez-Romero, P., A. Perez, A. Capul, R. Montgomery, and A. O. Fuller. 2005. Herpes simplex virus mediator associates in infected cells in a complex with viral proteins gD and at least gH. *J. Virol.* 79:4540–4544.
8. Perez-Romero, P., and A. O. Fuller. 2005. The C-terminus of the B5 receptor for herpes simplex virus contains a functional region important for infection. *J. Virol.* 79:7431–7437.
9. Perez, A., Q. Li, P. Perez-Romero, G. Delassus, S. R. Lopez, S. Sutter, N. McLaren, and A. O. Fuller. 2005. A new class of receptor for herpes simplex virus has heptad repeat motifs that are common to membrane fusion proteins. *J. Virol.* 79:7419–7430.
10. Connolly, S. A., D. J. Landsburg, A. Carfi, D. C. Wiley, R. J. Eisenberg, and G. H. Cohen. 2002. Structure-based analysis of the herpes simplex virus glycoprotein D binding site present on herpesvirus entry mediator HveA (HVEM). *J. Virol.* 76:10894–10904.
11. Nicola, A. V., J. H. Eugene, O. Major, and S. E. Straus. 2005. Herpes simplex virus type 1 enters human epidermal keratinocytes, but not neurons, via a pH-dependent endocytic pathway. *J. Virol.* 79:7609–7616.
12. Wild, C., T. Greenwell, and T. Matthews. 1993. A synthetic peptide from HIV-1 gp41 is a potent inhibitor of virus-mediated cell-cell fusion. *AIDS Res Hum. Retrovir.* 9:1051–1053.
13. Wild, C., D. C. Shugars, T. K. Greenwell, C. B. McDanal, and T. J. Mathews. 1994. Peptides corresponding to a predicted α-helical domain of human immunodeficiency virus type 1 gp41 are potent inhibitors of virus infection. *Proc. Natl. Acad. Sci. USA*. 91:9770–9774.
14. Yao, Q., and R. W. Compans. 1996. Peptides corresponding to the heptad repeat sequence of human parainfluenza virus fusion protein are potent inhibitors of virus infection. *Virology*. 223:103–112.
15. Rapaport, D., M. Ovadia, and Y. Shai. 1885. A synthetic peptide corresponding to a conserved heptad repeat domain is a potent inhibitor of Sendai virus-cell fusion: an emerging similarity with functional domains of other viruses. *EMBO J.* 22:5524–5531.
16. Lambert, D. M., S. Barney, A. L. Lambert, K. Guthrie, R. Medinas, D. E. Davis, T. Bucy, J. Erickson, G. Merutka, and S. R. Petteway, Jr. 1996. Peptides from conserved regions of paramyxovirus fusion (F) proteins are potent inhibitors of viral fusion. *Proc. Natl. Acad. Sci. USA*. 93:2186–2191.
17. Alexiev, U., I. Rimke, and T. Pöhlmann. 2003. Elucidation of the nature of the conformational changes of the EF-interhelical loop in bacterorhodopsin and of the helix VIII on the cytoplasmic surface of bovine rhodopsin: a time-resolved fluorescence depolarization study. *J. Mol. Biol.* 328:705–719.
18. Pöhlmann T., R. A. Böckmann, H. Grubmüller, B. Uchanska-Ziegler, A. Ziegler, and U. Alexiev. 2004. Differential peptide dynamics is

linked to major histocompatibility complex polymorphism. *J. Biol. Chem.* 279:28197–28201.

19. Bilsel, O., L. Yang, J. A. Zitzwitz, J. M. Beechem, and C. R. Matthews. 1999. Time-resolved fluorescence anisotropy study of the refolding reaction of the α-subunit of tryptophan synthase reveals nonmonotonic behavior of the rotational correlation time. *Biochemistry.* 38:4177–4187.
20. Mukhopadhyay, S., P. K. Nayak, J. B. Udgaonkar, and G. Krishnamoorthy. 2006. Characterization of the formation of amyloid protofibrils from barstar by mapping residue-specific fluorescence dynamics. *J. Mol. Biol.* 358:935–942.
21. Lakshmikanth, G. S., and G. Krishnamoorthy. 1999. Solvent-exposed tryptophans probe the dynamics at protein surfaces. *Biophys. J.* 77: 1100–1106.
22. Nesterov, E. E., J. Skoch, B. T. Hyman, W. E. Klunk. B. J. Backskai, and T.M. Swager. 2005. In vivo optical imaging of amyloid aggregates in brain: design of fluorescent markers. *Angew. Chem. Int. Ed.* 44: 5452–5456.
23. Vallotton, P., R. Hovius, H. Pick, and H. Vogel. 2001. In vitro and in vivo ligand binding to the 5–HT3 serotonin rReceptor characterised by time-resolved fluorescence spectroscopy. *ChemBioChem.* 2:205–211.
24. Gibson, A., K. Baburaj, D. E. Day, I. Verhamme, J. D. Shores, and C. B. Peterson. 1997. The use of fluorescent probes to characterize conformational changes in the interaction between vitronectin and plasminogen activator inhibitor-1. *J. Biol. Chem.* 272:5112–5121.
25. Wang, Y., and T. G. Goodson III. 2007. Early aggregation in prion peptide nanostructures investigated by nonlinear and ultrafast time-resolved fluorescence spectroscopy. *J. Phys. Chem. B.* 111:327–330.
26. Maciejewski, A., and R. P. Steer. 1986. Spectral and photophysical properties of 9,10-diphenylanthracene in perfluoro-*n*-hexane: the influence of solute-solvent interactions. *J. Photochem.* 35:59–69.
27. Bhaskar, A., G. Ramakrishna, Z. Lu, R. Twieg, J. M. Hales, D. J. Hagan, E. Van Stryland, and Theodore Goodson III. 2006. Investigation of two-photon absorption properties in branched alkene and alkyne chromophores. *J. Am. Chem. Soc.* 128:11840–11849.
28. Varnavski, O., L. Sukhomlinova, R. Twieg, and T. Goodson III. 2004. Ultrafast exciton dynamics in a branched molecule investigated by time-resolved fluorescence, transient absorption, and three-pulse photon echo peak shift measurements. *J. Phys. Chem. B.* 108:10484–10492.
29. Varnavski, O., G. Menkir, T. Goodson III, and P. L. Burn. 2000. Ultrafast polarized fluorescence dynamics in an organic dendrimer. *Appl. Phys. Lett.* 77:1120–1122.
30. Varnavski, O., J. C. Ostrowski, L. Sukhomlinova, R. J. Twieg, G. C. Bazan, and T. Goodson III. 2001. Coherent effects in energy transport in model dendritic structures investigated by ultrafast fluorescence anisotropy spectroscopy. *J. Am. Chem. Soc.* 124:1736–1742.
31. Xu, C., and W. W. Webb. 1996. Measurement of two-photon excitation cross sections of molecular fluorophores with data from 690 to 1050 nm. *J. Opt. Soc. Am. B.* 13:481–491.
32. Wang, Y., G. S. He, P. N. Prasad, and T. Goodson III. 2005. Ultrafast dynamics in multibranched structures with enhanced two-photon absorption. *J. Am. Chem. Soc.* 127:10128–10129.
33. De Rossi and U. Hermel. 1999. β-sheet recognition by time-resolved fluorescence spectroscopy. *Appl. Spec.* 53:505–509.
34. Mehboob, S., B. Luo, B. M. Patel, and L. W.-M. Fung. 2001. $\alpha\beta$-spectrin coiled coil association at the tetramerization site. *Biochemistry.* 40:12457–12464.
35. Piñeiro, A., A. Villa, T. Vagt, B. Koksch, and A. E. Mark. 2005. A molecular dynamics study of the formation, stability, and oligomerization state of two designed coiled coils: possibilities and limitations. *Biophys J.* 89:3701–3713.
36. Cooper, T. M., and R. W. Woody. 1990. The effect of conformation on the CD of interacting helices: a theoretical study of tropomyosin. *Biopolymers.* 30:657–676.
37. Lau, S. Y. M., A. K. Taneja, and R. S. Hodges. 1984. Synthesis of a model protein of defined secondary and quaternary structure. Effect of chain length on the stabilization and formation of two stranded α-helical coiled coils. *J. Biol. Chem.* 259:13253–13261.
38. Holtzer, M. M. E., and A. Holtzer. 1995. The use of spectral decomposition via the convex constraint algorithm in interpreting the CD-observed unfolding transitions of coiled coils. *Biopolymers.* 36:365–379.
39. Bode, K. A., and J. Applequist. 1997. Helix bundles and coiled coils in α-spectrin and tropomyosin: a theoretical CD study. *Biopolymers.* 42:855–860.
40. Nilsson, K. P. R., J. D. M. Olsson, F. Stabo-Eeg, M. Lindgren, P. Konradsson, and O. Ingana. 2005. Chiral recognition of a synthetic peptide using enantiomeric conjugated polyelectrolytes and optical spectroscopy. *Macromolecules.* 38:6813–6821.
41. Wang, Y., and T. Goodson III. 2007. Two-photon-excited time-resolved fluorescence studies on conformation and aggregation of amyloid peptides. *J. Am. Chem. Soc.* In press.
42. Latt, S. A., S. Brodie, and S. H. Munroe. 1974. Optical studies of complexes of quinacrine with DNA and chromatin: implications for the fluorescence of cytological chromosome preparations. *Chromosoma (Berl.).* 49:17–40.
43. Unruh, J. R., G. Gokulrangan, G. H. Lushington, C. Johnson, and G. S. Wilson. 2005. Orientational dynamics and dye-DNA interactions in a dye-labeled DNA aptamer. *Biophys. J.* 88:3455–3465.
44. Harms, G. S., W. L. Freund, and C. K. Johnson. 1998. Time-resolved fluorescence study of conformational dynamics in opioid peptides. *J. Phys. Chem. B.* 102:5004–5010.
45. Neyroz, P., B. Zambelli, and S. Ciurli. 2006. Intrinsically disordered structure of *Bacillus pasteurii* UreG as revealed by steady state and time-resolved fluorescence spectroscopy. *Biochem.* 45:8918–8930.
46. Homchaudhuri, L., S. Kumar, and R. Swaminathan. 2006. Slow aggregation of lysozyme in alkaline pH monitored in real time employing the fluorescence anisotropy of covalent labeled dansyl probe. *FEBS Lett.* 580:2097–2101.
47. Kallipolitou, A., D. Deluca, U. Majdic, S. Lakamper, R. Cross, E. Meyhofer, L. Moroder, M. Schliwa, and G. Woehlke. 2001. Unusual properties of the fungal conventional kinesin neck domain from *Neurospora crassa*. *EMBO J.* 22:6226–6235.
48. Krishna, T. R., M. Parent, M. H. V. Werts, L. Moreaux, S. Gmouh, S. Charpak, A. Caminade, J. Majoral, and M. Blanchard-Desce. 2006. Water-soluble dendrimeric two-photon tracers for in vivo imaging. *Angew. Chem. Int. Ed. Engl.* 45:4645–4648.
49. Beljonne, D., W. Weseleers, E. Zojer, Z. Shuai, H. Vogel, J. K. Pond, J. W. Perry, S. R. Marder, and J. L. Brédas. 2002. Role of dimensionality on the two-photon absorption response of conjugated molecules: the case of octupolar compounds. *Adv. Funct. Mater.* 12: 631–641.
50. Goodson, T. G. III. 2005. Optical excitations in organic dendrimers investigated by time-resolved and nonlinear optical spectroscopy. *Acc. Chem. Res.* 38:99–107.
51. Tripet, B., R. D. Vale, and R. S. Hodges. 1997. Demonstration of coiled-coil interactions within the kinesin neck region using synthetic peptides. *J. Biol. Chem.* 272:8946–8956.
52. Culham, D. E., B. Tripet, K. I. Racher, R. T. Voegele, R. S. Hodges, and J. M. Wood. 2000. The role of the carboxyl terminal α-helical coiled coil domain in osmosensing by transporter ProP of *Escherichia coli*. *J. Mol. Recognit.* 13:309–322.
53. Masui, R., T. Mikawa, and S. Kuramitsu. 1997. Local folding of the N-terminal domain of *Escherichia coli* RecA controls protein-protein interaction. *J. Biol. Chem.* 272:27707–27715.
54. West, M. J., H. M. Webb, A. J. Sinclair, and D. N. Woolfson. 2004. Biophysical and mutational analysis of the putative bZIP domain of Epstein-Barr virus EBNA 3C. *J. Virol.* 78:9431–9445.
55. Root, D., V. K. Yadavalli, J. G. Forbes, and K. Wang. 2006. Coiled-coil nanomechanics and uncoiling and unfolding of the superhelix and α-helices of myosin. *Biophys. J.* 90:2852–2866.
56. Carr, C. M., and P. S. Kim. 1993. A spring-loaded mechanism for the conformational change of influenza hemagglutinin. *Cell.* 73:823–832.

57. Leikina, E., C. Ramos, I. Markovic, J. Zimmerberg, and L. V. Chernomordik. 2002. Reversible stages of the low-pH-triggered conformational change in influenza virus hemagglutinin. *EMBO J.* 21: 5701–5710.

58. Lindgren, M., K. Sörgjerd, and P. Hammarström. 2005. Detection and characterization of aggregates, prefibrillar amyloidgenic oligomers, and protofibrils using fluorescence spectroscopy. *Biophys. J.* 88:4200–4212.

59. Pandya, M. J., G. M. Spooner, M. Sunde, J. R. Thorpe, A. Rodger, and D. N. Woolfson. 2000. Sticky-end assembly of a designed peptide fiber provides insight into protein fibrillogenesis. *Biochemistry.* 39:8728–8734.

60. Larson, D. R., W. R. Zipfel, R. M. Williams, S. W. Clark, M. P. Bruchez, F. W. Wise, and W. W. Webb. 2003. Water-soluble quantum dots for multiphoton fluorescence imaging in vivo. *Science.* 30:1434–1436.

61. Zhou, W., S. M. Kuebler, K. L. Braun, T. Yu, J. K. Cammack, C. K. Ober, J. W. Perry, and S. R. Marder. 2002. An efficient two-photon-generated photoacid applied to positive-tone 3D microfabrication. *Science.* 296:1106–1109.

62. Mongin, O., L. Porrès, T. Pons, C. Katan, J. Mertz, and M. Blanchard-Desce. 2003. Synthesis and two-photon absorption of highly soluble three-branched fluorenylene-vinylenederivatives. *Tetrahedron Lett.* 44:8121–8125.

63. Pan, O., and K. Beck. 1998. The C-terminal domain of matrilin-2 assembles into a three-stranded α-helical coiled coil. *J. Biol. Chem.* 273:14205–14209.

64. Heimburg T., J. Schünemann, K.Weber, and N. Geisler. 1999. FTIR-spectroscopy of multistranded coiled coil proteins. *Biochemistry.* 38: 12727–12734.

65. Burkhard, P., S. Ivaninskii, and A. Lustig. 2002. Improving coiled-coil stability by optimizing ionic interactions. *J. Mol. Biol.* 318:901–910.

66. Kundu, B., N. R. Maiti, E. M. Jones, K. A. Surewicz, D. L. Vanik, and W. K. Surewicz. 2003. Nucleation-dependent conformational conversion of the Y145Stop variant of human prion protein: structural clues for prion propagation. *Proc. Natl. Acad. Sci. USA.* 100:12069–12074.

67. Estes D., S. R. Lopez, A. O. Fuller, and M. Mayer. 2006. Triggering and visualizing the aggregation and fusion of lipid membranes in microfluidic chambers. *Biophys. J.* 91:233–243.